University of Baghdad
College of Engineering
JOURNAL OF ENGINEERING

Journal of Engineering

journal homepage: www.jcoeng.edu.iq

Volume 32 Number 5 May 2026

Electronic Circuit Design and Modeling of Biodegradable Mxene-Based Wireless Biosensor for Deep Wound Monitoring

Zainab Hussam AL-Araji [1, *], **Nada A. Swaikat** [2]

[1]Physics Department, College of Science for Women, University of Baghdad, Baghdad, Iraq
[2]Voronezh State Technical University, 394000, Voronezh, Russia

ABSTRACT

One of the most significant challenges of medical care is the infection of postoperative wounds, and conventional visual examination often fails to detect it early. This research proposes the design of an innovative, passive wireless telemetry system for non-intrusive monitoring of the wound-healing process . The system integrates a biocompatible resonance circuit (LC) with a high-sensitivity piezoresistive sensor based on MXene ($Ti_3C_2T_x$). It operates within the standard industrial and medical (ISM) band at 13.56 MHz.The detection mechanism in the system is based on the principle of "impedance modulation" (Impedance Modulation), which arises from changes in the sensor's resistance under physiological tissue pressure. The system was modeled and simulated using the Proteus environment to evaluate its frequency response. The results showed a high dynamic range, as the system recorded a stable output voltage of 863 mV (-1.28 dB) during the recovery phase (Rs≈10KΩ), against a sharp decrease to 15 mV (-36.5 dB) during the inflammation phase (Rs≈100Ω), which effectively indicates the phenomenon of "signal breakdown". In addition, sensitivity analysis emphasized the importance of component compatibility, as an amplitude mismatch caused the resonance frequency to shift to 11.9 MHz. The proposed system can accurately distinguish between healthy and inflamed tissues.

Keywords: Biodegradable electronics, MXene $Ti_3C_2T_x$, Passive wireless telemetry, Transient implants.

1. INTRODUCTION

Traditional visual inspection lacks objectivity, increasing the risk of contamination, necessitating the development of a "smart bandage" for continuous monitoring **(Pang et al., 2023; Dong et al., 2024)**. Despite the accuracy of active electronic systems, relying on batteries is a major drawback; it imposes weight restrictions and undermines the flexibility needed to align the body's curves **(Derakhshandeh et al., 2018; Mostafalu et al., 2018)**. And, as pointed out by **(Xu et al., 2019)**, even more dangerous is the biological risk posed by the potential leakage of toxic electrolytes from batteries into soft tissues, rendering these

*Corresponding author
Peer review under the responsibility of University of Baghdad.
https://doi.org/10.31026/j.eng.2026.05.01

Article received: 03/01/2026
Article revised: 28/03/2026
Article accepted: 11/04/2026
Article published: 01/05/2026

systems unsuitable for long-term implantation **(Song et al., 2021).** As a safe alternative, passive wireless telemetry technology has emerged that dispenses with batteries. In this context, **(Boutry et al., 2019)**, a pioneering model of a fully biodegradable sensor using magnesium coils. Although biocompatibility was achieved, the physical drawback of the poor electrical conductivity of biodegradable materials compared to noble metals (such as gold and copper) led to a sharp decrease in the quality factor (Q-Factor), which significantly reduced the readability and sensitivity of the system, as confirmed by **(Zhang et al., 2020)**. Recently, two-dimensional nanomaterials, specifically the MXene family (MXene $Ti_3C_2T_x$), have come into the spotlight due to their unique properties, combining metallic conductivity with a hydrophilic surface **(Soleymaniha et al., 2023; Murali et al., 2021).**

Studies by **(Guo et al., 2018; Ma et al., 2020)** prove that MXene sensors are superior to piezoresistive sensors in terms of high sensitivity to micro-mechanical stimuli. However, the vast majority of these applications were limited to wearable devices (Wearables) or relied solely on detecting "frequency Shift", a mechanism that requires complex and expensive spectrum analyzers to read, which limits their feasibility in home care environments or simple clinics.

The fundamental research gap that lies in the absence of a system that combines:
(1) complete biocompatibility,
(2) High sensitivity to nanomaterials,
(3) the simplicity of the electronic reading mechanism.

Therefore, this research aims to design and simulate a hybrid passive wireless telemetry system operating within the bandwidth (ISM 13.56 MHz). The original scientific contribution of this work is to exploit the significant variation in the resistance of the MXene sensor to induce (Resonance Amplitude Modulation) rather than the traditional dependence on frequency displacement. This proposed methodology provides a clear binary response that accurately distinguishes between the state of "physiological stability" and the state of" inflammatory risk, paving the way for the development of intelligent, low-cost, battery-free medical implants. of intelligent, low-cost, battery-free medical implants.

2. METHODOLOGY AND SYSTEM DESIGN

In this paper, we propose a passive wireless telemetry system to monitor pressure inside surgical wounds without the need for batteries or wires that penetrate the skin **(Tan et al., 2020; Nguyen et al., 2019)**. **Fig. 1** shows that the system consists of two functional units:

1-External Reader Unit: It is a serial resonant circuit (L1, C1) that serves as both a power source and a data receiver, generating an oscillating magnetic field at 13.56 MHz.
2-Implantable sensor Unit: it is an entirely passive parallel-resonance circuit (L2, C2) that integrates an inductive coil with an MXene sensor acting as a variable resistor (Rs).

The proposed design is based on the principle of inductive Coupling, in which a change in tissue pressure (caused by swelling or inflammation) alters the resistance of the MXene-piezo resistance sensor, thereby modifying the quality factor (Q-factor) of the implanted circuit. This adjustment is immediately reflected in the" input impedance " in the external reader via the wireless link, which makes it possible to detect the pathological condition **(Mirbozorgi et al., 2016).**

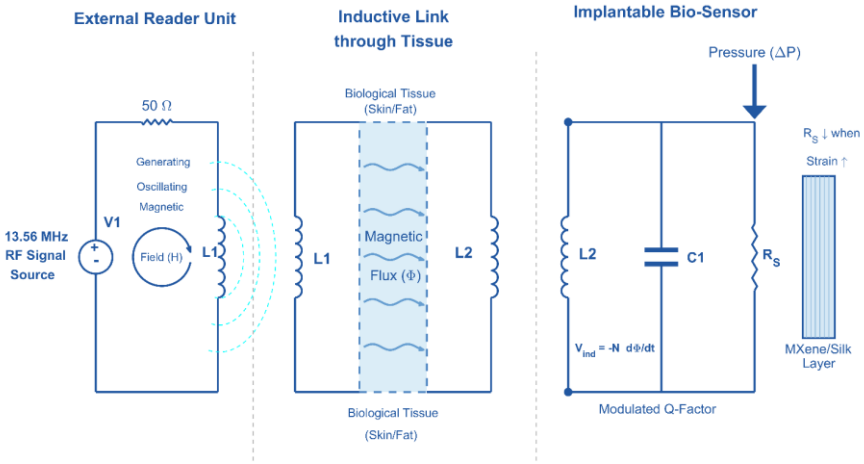

Figure 1. The conceptual scheme of the passive wireless telemetry system, explaining the mechanism of inductive coupling between the external reader and the implanted sensor, and the effect of the MXene impedance (Rs) on the signal.

2.1 Theoretical Framework

To ensure that the system complies with physical medical standards and design accuracy, the governing equations of circuit behavior were derived before the simulation began. Resonance frequency and transmission parameters according to a study by **(Yates et al., 2017),** the system is tuned to operate within the medical and scientific band (ISM Band) at a frequency of 13.56 MHz. This frequency is optimal for short-term implant applications, as it achieves a balance between tissue penetration and reduced energy absorption (SAR). The resonance frequency of the implanted circuit is calculated according to the Thomson equation:

$$f_0 = \frac{1}{2\pi\sqrt{L_2 C_{res}}} \tag{1}$$

Where L_2 is the inductance of the implanted coil, and C_{res} The capacitance of the capacitor. This value must accurately match the reader's frequency to ensure maximum power transfer.

2.2 Reflected Impedance Analysis

This part represents the physical essence of the detection process. The effect of the implanted sensor on the external reader can be modeled by the "reflected impedance." Z_{ref} that appears in the reader file, given by the following equation **(RamRakhyani et al., 2011):**

$$Z_{ref} = \frac{(\omega M)^2}{Z_{sensor}} \tag{2}$$

Where, ω angular frequency, Mutual inductance between the two coils depends on the coupling coefficient $M = k\sqrt{L_1 L_2}$,Z_{sensor}. The total impedance of the implanted circuit, which includes the MXene resistance Rs.

2.3 Sensor Design

To achieve biocompatibility requirements, the sensor is designed with a multilayer structure, as shown in the explosion diagram in **Fig. 2.** The proposed design consists of the following materials:

1. Biodegradable Substrate: made of "silk Fibroin" **(Xu et al., 2023)** with a thickness of ≈ 30 µm, a material that provides mechanical support and biodegrades without inducing a negative immune response.
2. Telemetry Coil: it is designed using magnesium (Mg) with a thickness of 150 µm, due to its good conductivity and solubility in bio-liquids **(Li et al., 2022).**
3. Active Sensing Area: consists of a MXene/silk composite with an interdigitated pattern, to ensure high pressure sensitivity.
4. Protective Encapsulation Layer: silk top layer to protect the circuit and control the time decomposition rate.

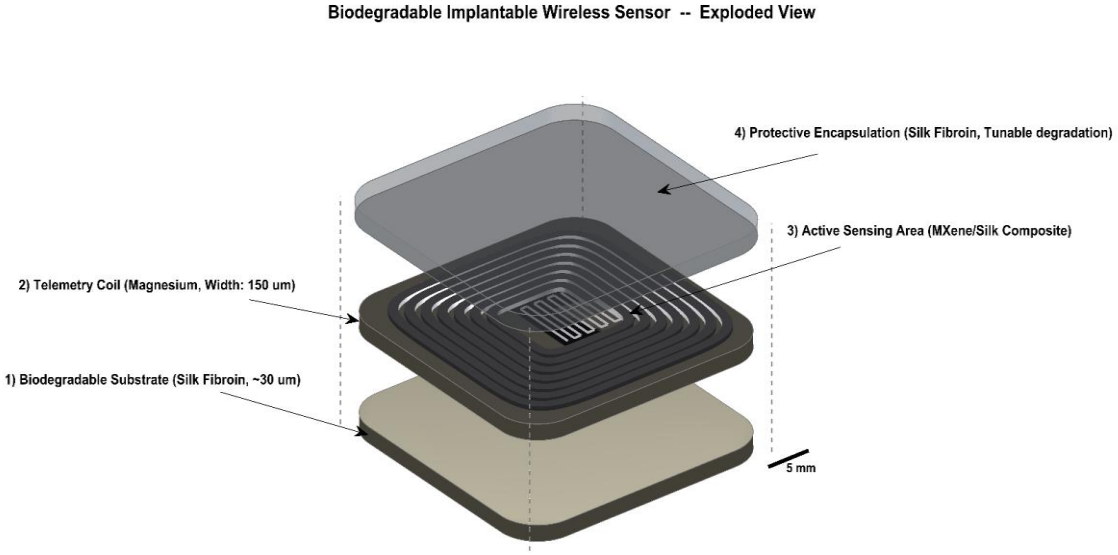

Figure 2. The multilayer structure of the proposed sensor

2.4 Wireless Metering Mechanism: Inductive Coupling and Reflected Impedance

The wireless communication link is created via Near-Field inductive coupling between the external reader coil (L1) and the implanted sensor coil (L2). Since the sensor is passive (battery-free), it operates in the "reactive near field" at 13.56MHz. The efficiency of this link is subject to mutual induction (M), which is calculated as follows:

$$M = k\sqrt{L_1 L_2} \tag{3}$$

$$Z_{in} = Z_1 + \frac{(\omega M)^2}{Z_{sensor}} \tag{4}$$

$$Z_{in} = (R_1 + j\omega L_1) + \frac{(\omega M)^2}{R_s + j\left(\omega L_2 - \frac{1}{\omega C_{res}}\right)} \tag{5}$$

where k is the coupling coefficient, the basic detection principle is based on" reflected impedance, where changes in the impedance of the sensor (Zsensor) caused by wound healing (change RS) are reflected to the primary reader circuit. The above equation expresses the equivalent income impedance seen by the reader (Zin). This equation shows

that any change in the wound's vital impedance directly modifies the external reader's input impedance, causing a detectable shift in the output voltage.

2.5 Simulation Setup and Frequency

To ensure the accuracy of the results and to verify the sensitivity of the proposed wireless telemetry system to the components, the simulation was conducted using the Proteus Design Suite. A comparative analysis was performed using two different, distinct resonant capacitance Cres scenarios to assess the impact of the frequency tuning on signal integrity :

1. Standard Detubed Case (100 PF): The purpose of this setup is to study the behavior of the circuit with common commercial values and to observe the effect of a frequency shift F0=11.86 MHz caused by an exact mismatch in the coil inductance (1.8 mH).
2 .Tuned \ Case: the capacitor capacitance is precisely set at 76.5 pF based on the resonance equation Eq. (1), to ensure that the system works exactly at the target medical frequency of 13.56 MHz and achieves maximum energy transfer efficiency.

In both settings, the bio-degradable MXene sensor was modeled as a variable resistor (100, k1, 10 k) and used to monitor differences in frequency response and signal amplitude, as well as the output voltage Vout and the Quality Factor Q.

Table 1. Design specifications and simulation parameters of the proposed wireless telemetry system

Category	Parameter	Symbol	Value
system space	Operating frequency(ISM)	f_0	13.56 MHz
	Coupling coefficient	k	0.15
	working distance	d	10-20 mm
Reader Unit (Tx)	Primary Inductance	L_1	1.8 mH
	Primary Capacitance	C_1	76.5 pF
	Source Impedance	R_{source}	50 Ω
Sensor Unit (Rx)	Secondary Inductance (Mg)	L_2	1.8 mH
	Coil Thickness	t_{coil}	150μm
Tuning Cases	**Case A**		
	Resulting Frequency	F_A	11.86 MHz
	Resonant Capacitance	C_{res}	100 pF
	Case B		
	Resulting Frequency	F_B	13.56 MHz
	Resonant Capacitance	C_{res}	76.5 pF
MXene Sensor	Inflammation Resistance Proliferation Resistance Remodeling Resistance	R_S	100Ω-1KΩ-10KΩ

3. DIAGNOSTIC ALGORITHM AND CLINICAL DECISION-MAKING STRATEGY

To bridge the gap between wireless measurements and clinical practice, a quantitative Triage Algorithm has been developed that uses the voltage gain (Av) to determine the healing stage with high accuracy, thereby minimizing the risk of diagnostic errors. The proposed system works according to a three-tier Triage Algorithm, as shown in the decision matrix **Fig. 3**, where the wound condition is classified into three distinct diagnostic zones based on the value of the received output voltage (Vout) at the resonance frequency:

1. Zone I: Critical Intervention Zone Quantitative Indicator:

- Signal Amplitude Breakdown $V_{out} \leq 20mV$, $Gain < -30\ dB$

- Physiological correlation: this sharp decrease reflects a decrease in the sensor's resistance at low levels (Rs = 100Ω) due to high mechanical Strain. Medically, this is associated with severe edema (Severe Edema) or the accumulation of dense exudates (Exudates), both of which are vital indicators of the onset of infection (Infection Onset) or the occurrence of internal bleeding.

- Clinical protocol: the system classifies the condition as "high-risk". A mandatory medical procedure is to remove the bandage for direct visual inspection immediately, perform debridement (removal of dead tissue) of the wound, and start an antimicrobial therapy protocol.

2. Zone II: Active Monitoring & Recovery Zone

- Quantitative indicator: average signal response $100 < V_{out} < 500mV$, $Gain \approx -16\ dB$
- Physiological correlation: a gradual improvement in the output voltage indicates a high resistance of the sensor (Rs ≈1 k) as a result of the regression of swelling and the onset of the stage of cellular proliferation. At this stage, granulation Tissue (Granulation Tissue) begins to form, reducing pressure on the sensor.
- Clinical protocol: the system classifies the condition as "stable/Healing". Protocol recommends adopting a "non-intervention" strategy, in which the bandage should be kept closed to maintain a moist, sterile wound environment.

3. Zone III: Full Recovery (Healed Zone),

- Quantitative indicator: voltage: $V_{out} \geq 800mV$, $Gain > 0\ dB$ (positive gain)
-Physiological correlation: the arrival of the gain to positive values means that the transmission system works with maximum efficiency as a result of the sensor returning to its normal physical state (Rs =10k). This confirms the healing stage.
- Clinical protocol: when the system shows an indicator of pain relief and treatment success, the decision is to end electronic monitoring and remove the smart bandage. Table 2 shows the proposed diagnostic framework. This table accurately relates the electrical parameters derived from the simulation (Rs, Vout, gain) to the physiological stages of wound healing, thereby determining the quantitative thresholds needed to guide medical decisions.

Table 2. The proposed diagnostic protocol correlating electrical parameters with clinical Action.

Diagnostic Zone	**Sensor Resistance (Rs)**	**Output Voltage (Vout)**	**Voltage Gain (dB)**	**Physiological State**	**Clinical Decision**
Zone I (Danger)	Low Rs ≈ 100Ω	$V_{out} \leq 20mV$	$Gain < -30\ dB$	Severe Edema / Infection	Intervention (Open & Treat)
Zone II (Healing)	Medium Rs ≈1 k	$100 < V_{out} < 500mV$	$Gain \approx -16\ dB$	Tissue Proliferation	Monitor (Keep Closed)
Zone III (Healed)	High Rs ≈10k	$V_{out} \geq 800mV$	$Gain > 0\ dB$	Remodeling / Normal Skin	Discharge (Remove Sensor)

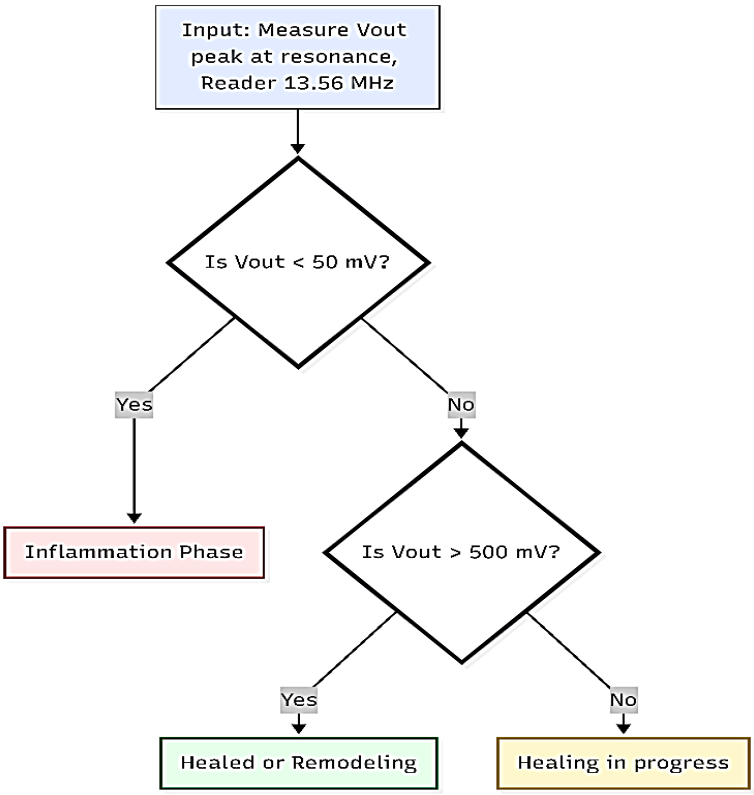

Figure 3. Flowchart of the proposed quantitative sorting algorithm. The diagram shows the logical decision-making process for classifying the wound condition.

4. RESULTS AND DISCUSSION

To evaluate the performance of the proposed wireless system through a series of simulation scenarios aimed at verifying frequency response, Dynamic Sensitivity to bio-impedance changes, and design durability against component unevenness. All numerical results were interpreted by direct reference to the mathematical model of the equivalent circuit (ECM) and the documented physical foundations **(Ghaffar et al., 2015).**

4.1 Validation, Resonance Tuning, And System Efficiency

To verify the conformity of the operating frequency with the medical standard intended for medical and industrial devices (ISM Band) **(Yates et al., 2017).** Frequency-Response simulation (AC Sweep) of the circuit was performed in its ideal state (without a pressure load), and the results showed that this results in the correctness of the calculations derived from equation (1) given in the methodology **(RamRakhyani et al., 2011)**:

$$f_0 = \frac{1}{2\pi\sqrt{1.8\mu H \times 76.6pF}} \approx 13.56MHz \quad (6)$$

The output voltage (Vout) as shown in **Fig. 4** as a function of frequency. The simulation showed that using a precise resonance amplitude (Cres = 76.5 pF) and the calculated inductance (Ls = 1.8 mu) cancelled the capacitive and inductive mutual reactance, resulting in a sharp resonance peak at exactly the target frequency. It confirms the correctness of theoretical calculations and ensures the maximum efficiency of Energy Transfer in accordance with the principles of the near-field coupling types used in modern medical implants.

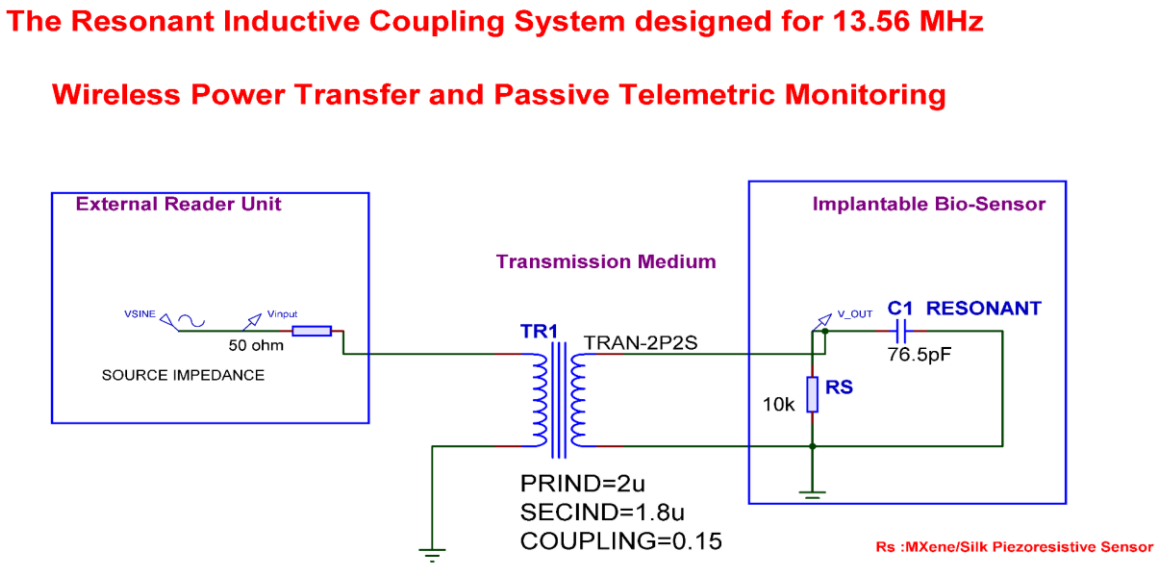

Figure 4. Schematic diagram of the proposed wireless system. The figure shows the external reading phase and the implanted phase, consisting of an induction (magnesium) and a Maxine/silk (Rs) sensor, in which the circuit (LC Tank) was set to operate at the central frequency of 13.56 MHz.

4.2 Dynamic Response to the Stages of Wound Healing

The sensor's sensitivity to physiological changes was tested by varying the load resistance Rs to represent different healing stages, based on the clinically proven inverse relationship between tissue moisture and bioelectric resistance (Bio-impedance) **(Gao et al., 2023).** The results in **Figs. 5 to 7** indicate three distinct cases:

4.2.1 The Inflammatory Phase (Danger)

When simulating a wet edema environment and reduced skin resistance (Rs= 100), as confirmed by clinical studies on chronic wound impedance **(Lonini et al., 2018; Derakhshandeh et al., 2018),** the output voltage dropped sharply to a record low of 15 mV, indicating a state of "signal breakdown". This is attributable to over-dumping, in which low resistance degrades the quality factor (Q), preventing the formation of stable oscillation. This response provides an immediate diagnostic indication of complications.

4.2.2 The Stage of Reproduction (Recovery)

As the tissues recovered and their resistance rose, Rs =10 k as a result of drying of secretions and restoration of the stratum corneum **(Gurtner et al., 2008)**. The system restored its stable Oscillation and recorded a peak voltage of 863 =mV, reflecting the return of tissues to their normal insulating properties.

4.2.3 The Stage of Remodeling (Healing)

In the final state (Rs = 10 k), the voltage reached its peak (836 mV), confirming the restoration of the skin's insulating properties.

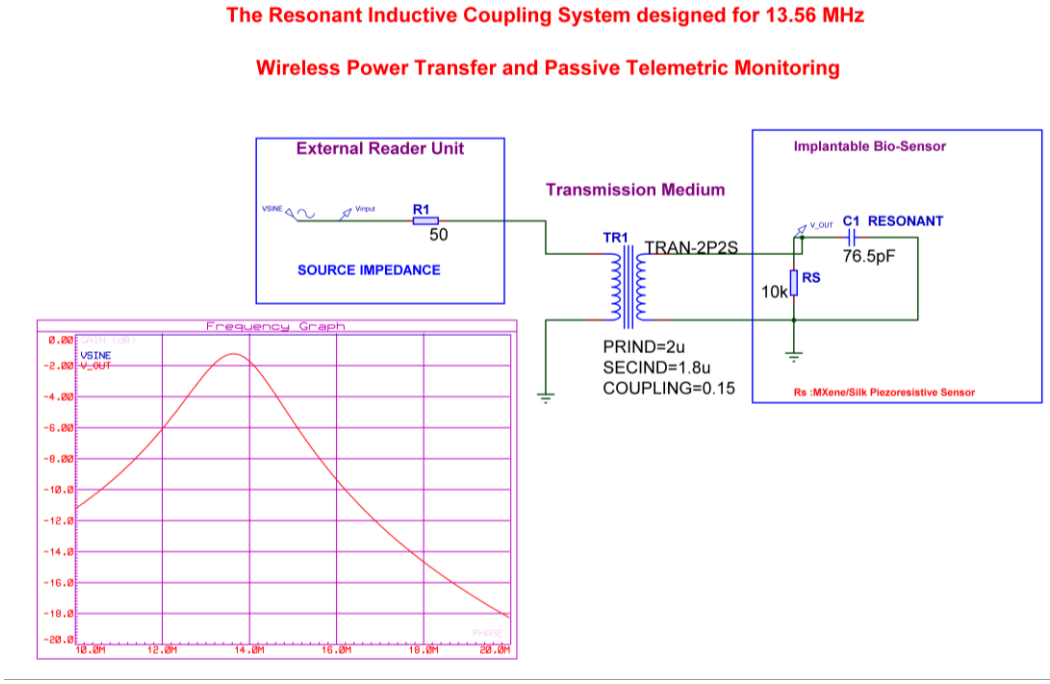

(a)

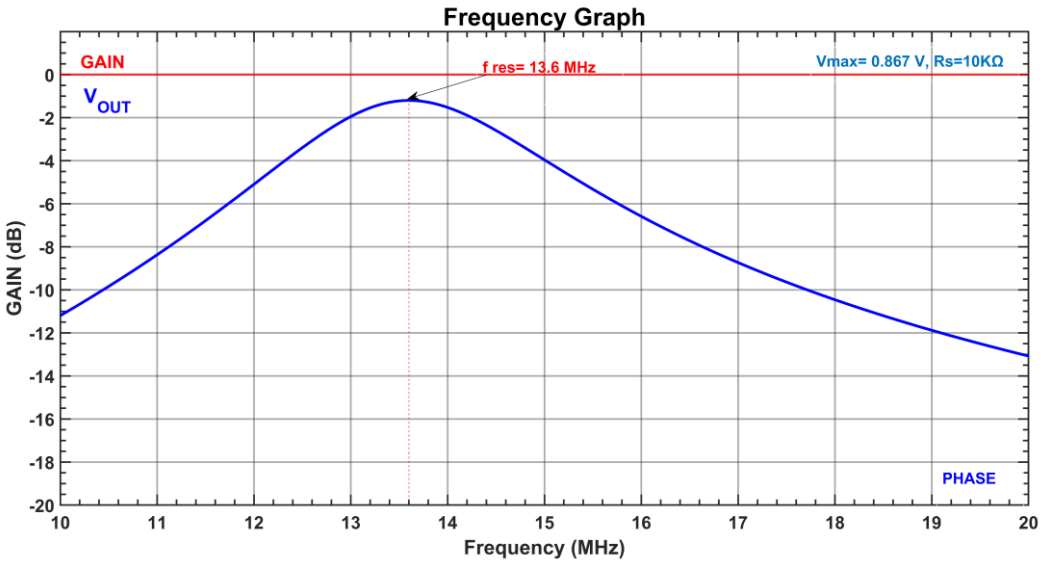

(b)

Figure 5. The system response indicates complete tissue healing (Rs = 10 k). Both (a) the circuit diagram and (b) the corresponding frequency curve demonstrates the restoration of ideal resonance performance.

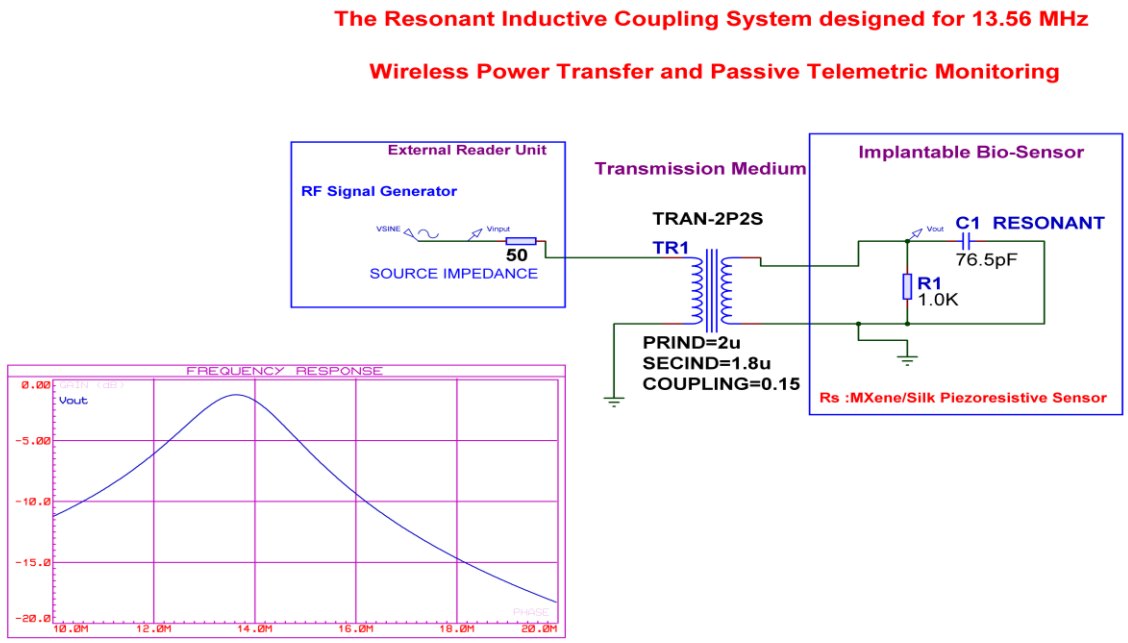

(a)

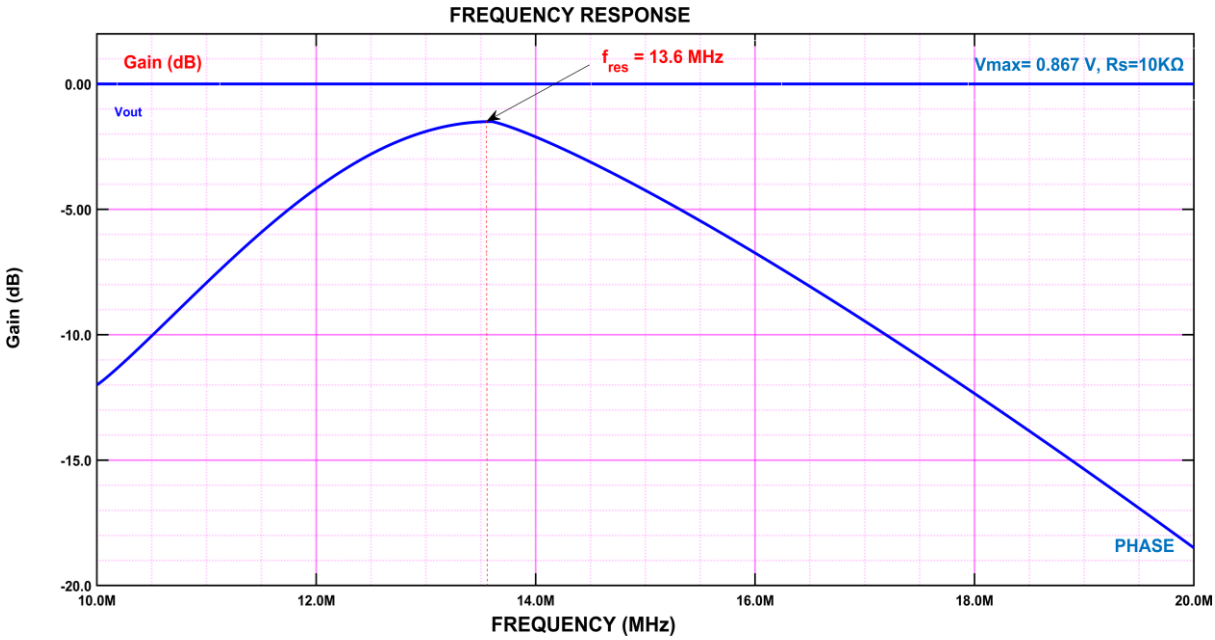

(b)

Figure 6. The system response is indicative of complete tissue healing (Rs = 1 k). Both (a) the circuit diagram and (b) the corresponding frequency curve demonstrates the restoration of indicating the onset of tissue healing.

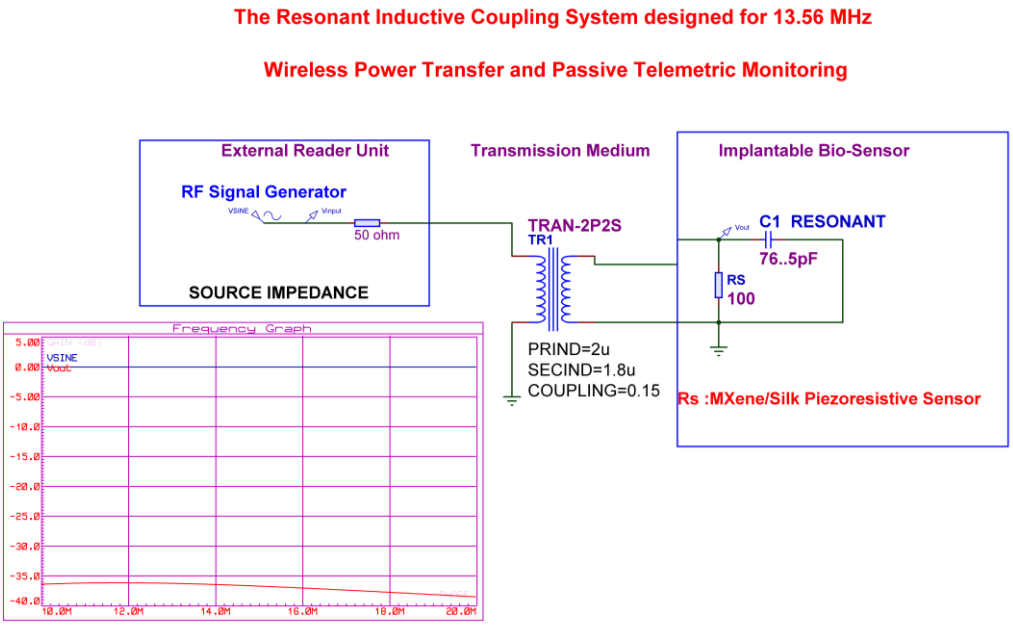

(a)

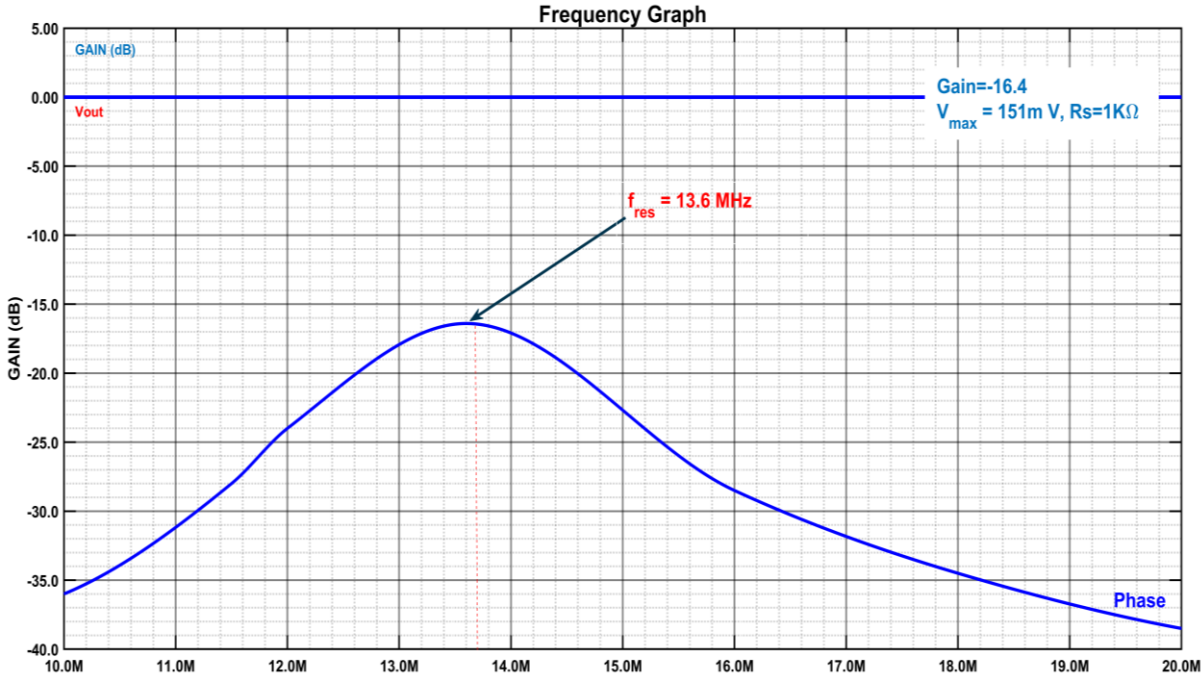

(b)

Figure 7. The system response is indicative of complete tissue healing (Rs = 100). Both (a) the circuit diagram and (b) the corresponding frequency curve demonstrate the Inflammation Phase.

The simulation results are shown in **Figs. 5-7** confirm the nonlinear centrifugal relationship between tissue uniformity of healing and signal transmission efficiency.

The system shows a wide dynamic range:

1. The output voltage jumps from a critical level of 15t mV during the wet Inflammation phase.

2. To multiply more than 57 times and reach 867mv when fully cured.

To provide a holistic view of system performance, the frequency responses of the three main healing phases are combined within this comparative framework; **Fig. 8** shows the dynamic path of the output voltage, starting from the "signal collapse" state associated with acute inflammation, up to the complete restoration of the signal during the reconstruction phase. This sharp contrast in response is conclusive evidence of the sensor's superior ability to accurately distinguish overlapping healing phases, cementing its position as a reliable tool for continuous clinical monitoring.

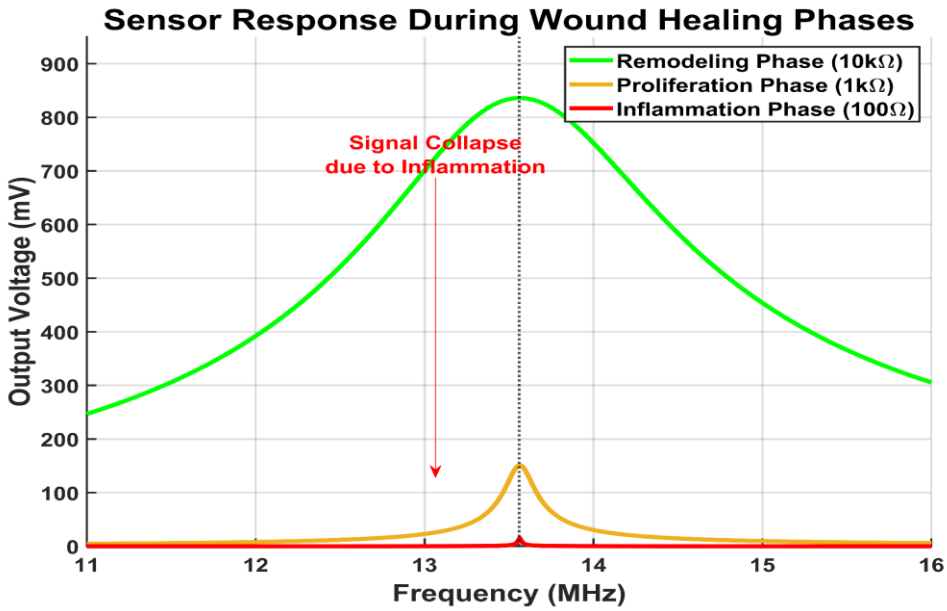

Figure 8. Dynamic frequency response across the three stages of healing (inflammation, proliferation, and reconstruction).

4.3 The Effect of Changing Electronic Components on the Sensitivity of the System

To evaluate manufacturing robustness, the ideal synthesis option (C = 76.5 pF), which accurately maintained a resonance at 13.56 MHz, was compared with the capacitance (C = 100 pF) .The response curve in **Fig. 9** shows a frequency shift of about 11.56 MHz, demonstrating the system's high sensitivity to manufacturing errors. Therefore, in this test, a standard tolerance deviation was introduced in the resonant capacitance value (Cres) as illustrated in **Fig. 9** to simulate these deviations, to study their effect on the stability of the resonant frequency and determine the extent to which the system remains within the external reader's effective operational bandwidth **(RamRakhyani et al., 2011).** The response curve shows a frequency shift of about 11.56 MHz, demonstrating the system's

high sensitivity to Cres manufacturing errors and highlighting the need for precision fabrication techniques.

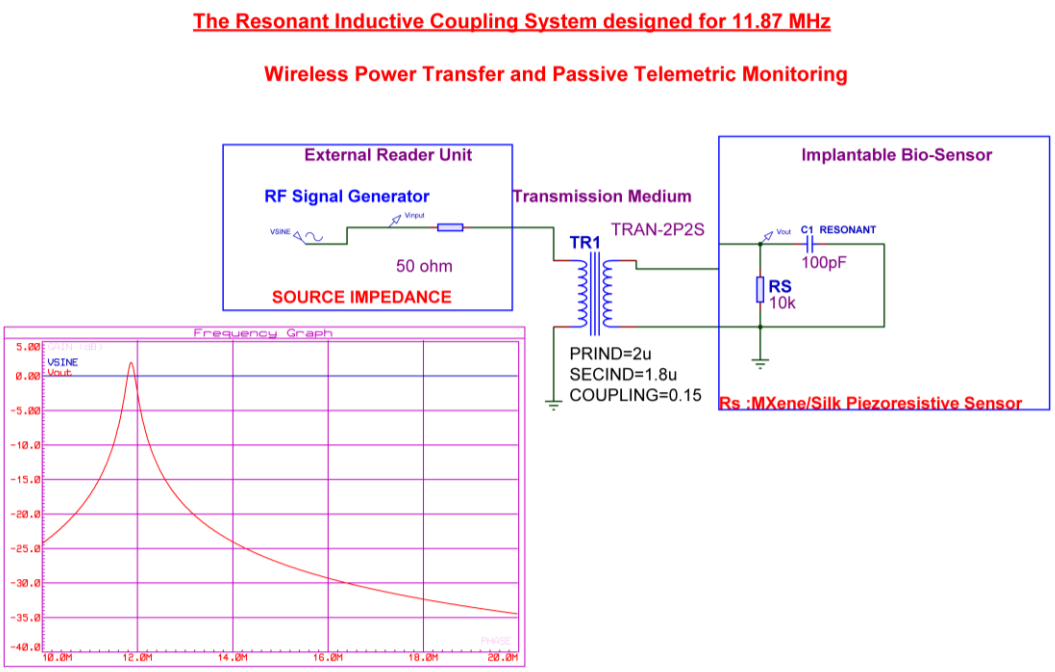

(a)

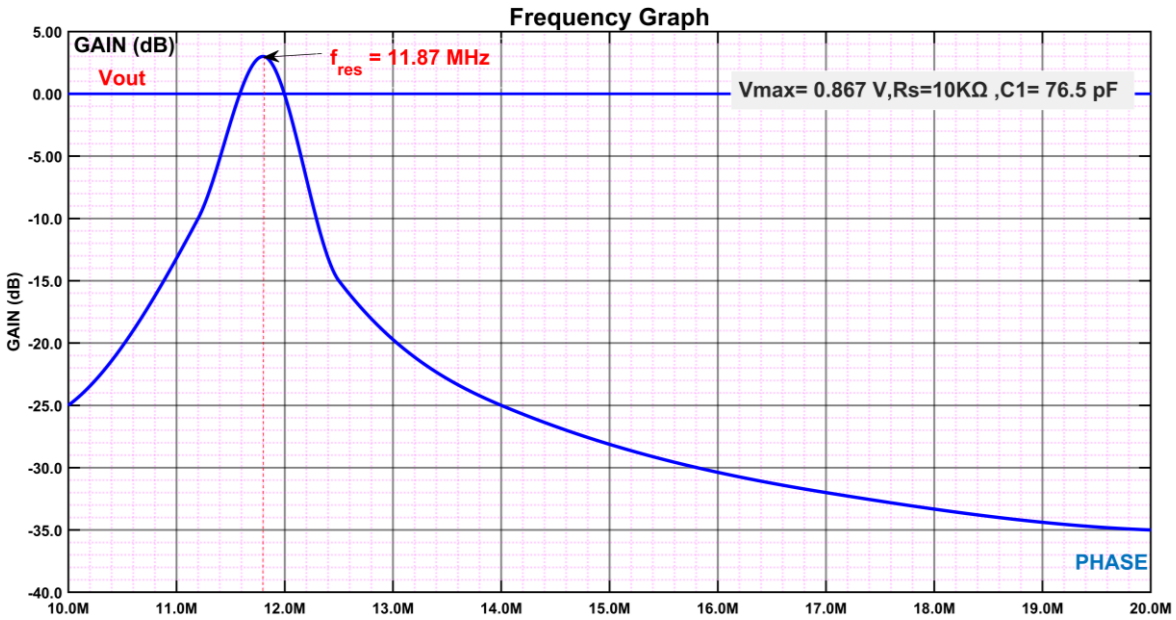

Figure 9. The resonance is detuning due to capacitance variation (C1= 76.5 pF). (a) the circuit diagram and (b) the corresponding frequency curve demonstrates the Inflammation Phase.

4.4 Predictive Modeling of Hydrolysis and Operational Life

Based on the methodology of "transient electronics" (Transient Electronics), a numerical model has been developed to simulate the corrosion and porosity of magnesium **(Yang et al., 2022)**. The model was based on the kinetics of hydrolysis of magnesium in the physiological medium (pH=7.4) according to the reaction:

$$Mg + 2H_2O \rightarrow Mg(OH)_2 + H_2$$

Consistent with the kinetics of electrochemical corrosion of magnesium in physiological media **(Witte et al., 2005), Fig. 10** shows an inverse relationship between implantation time and device performance. The curve shows a linear decrease in the quality factor (Q) as the coil's cross-sectional area decreases, limiting the "safe operating window" to 10 days. By the fourteenth day, the device reaches full functional fading, which closely aligns with the clinical schedule for healing acute wounds **(Gurtner et al., 2008)** and aligns with the principle of "programmed transience" established in research on transient electronics **(Hwang et al., 2012)**. Although this work focuses on electronic design, the materials were carefully selected to ensure biological compliance. The breakdown products of magnesium (Mg) are natural electrolytes that are safely absorbed by the body and do not exceed the recommended daily dose, which reduces the risk of systemic toxicity **(Lin et al., 2021)**. In addition, the silk Fibroin substrate and the Maxine sensor provide an isolation that prevents a chronic inflammatory response, as recent studies have demonstrated the high cellular compatibility of these substances and their non-causation of oxidative stress **(Zhu et al., 2016; Huang et al., 2019). Fig.10** illustrates the complete disappearance of the organ, eliminating the risk of long-term fibrosis. Finally, to highlight the advantages and novelty of the developed sensor based on MXene, **Table 3** presents a comparative analysis of the latest research on wound monitoring systems with the proposed work

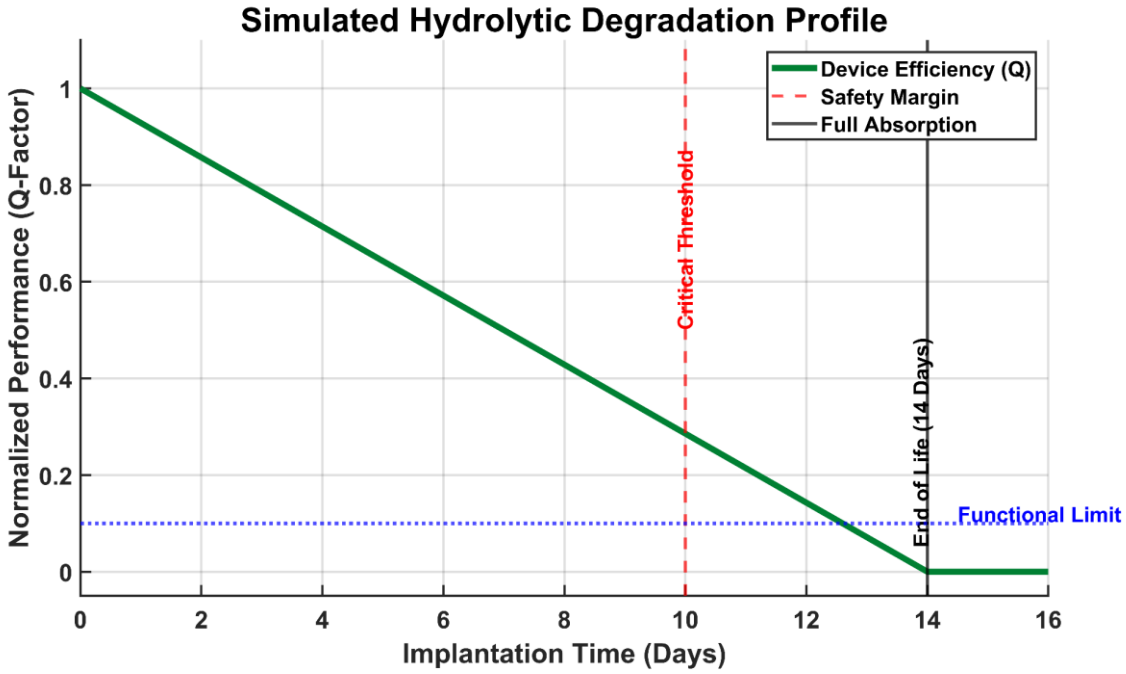

Figure 10. The hydrolysis diagram shows the linear decrease of the quality factor (Q-factor) and the persistence of functional efficacy up to day 12.6, ensuring coverage of the critical recovery period before complete hydrolysis (day 14)

Table 3. Comparative analysis of the latest research on wound monitoring systems with the proposed work

Reference	Sensing Material	Operation and Power	Readout Parameter	Critical Limitation / Gap	Proposed Contribution
(Mostafalu et al., 2018)	Si-based	Active It requires a battery and a microcontroller	Digital data	System rigidity and toxic batteries reduce elasticity and pose a risk of toxic substance leakage (Cytotoxicity).	Passive Completely battery-free and based on magnetic induction.
(Boutry et al., 2018)	Mg/PLA	Passive The RLC circuit is biodegradable.	Frequency shift	Low Q-Factor Poor conductivity of biodegradable materials significantly reduces the reading range and sensitivity.	Superconductivity: The use of MXene ensures a high Q-factor and high sensitivity, despite the absence of a battery.
(Luo et al., 2019)	Graphene Foam	Passive Strain.	Frequency shift	Hydrophobicity makes it difficult for the sensor to stick to wet tissues, which causes the sensor to slip Motion Artifacts.	Hydrophilic MXenee contains functional groups (OH) that are biofused with moist tissues.
(Guo et al., 2020)	$Ti_3C_2T_x$	Passive Humidity/pressure sensor.	Frequency shift	Readout Complexity It requires detecting very small or very minor frequency changes ,which necessitates expensive and clinically impractical VNA spectrum analyzers.	Capacity adjustment Converting pressure into a voltage breakdown (from 863 mV to 15 mV) can be done with a simple, inexpensive circuit.
(Wang et al., 2023)	CNTs	Passive	Resistance change	Biosafety has a high potential for toxicity and cell damage upon long-term direct contact.	The use of silk substrate (Silk) and bio-safe MXene.
This Work	MXene/ Silk	Passive Wireless ISM Band 13.56 MHz	Amplitude Modulation	--	Binary Outcome It provides a categorical distinction between "safety" and" danger " with a very high voltage contrast (-36 dB drop).

5. CONCLUSIONS

This research provides an engineering basis for the development of transient electronics by modeling a fully biodegradable wireless sensor system. By integrating a Maxine-based compression pressure sensor MXene ($Ti_3C_2T_x$), into a resonance circuit (LC) operating at a frequency of 13.56 MHz. The proposed system demonstrated high accuracy in signal transmission by adjusting impedance. The simulation results have confirmed the presence

of a wide dynamic range responsive to physiological changes, in which the voltage rises from the baseline of 15 mV (during acute inflammation and with a resistance of 100 Ω) to a peak of 863 mV (during histological reconstruction and with a resistance of 10 KΩ).In addition, the proposed "quantitative sorting algorithm" bridged the gap between raw voltage data and medical decision-making, turning subtle discrepancies into specific clinical categories (critical, transitional, safe). While the sensitivity analysis showed the need to adhere to high-precision manufacturing to avoid capacitance detuning, the compatibility of the functional life of the system (12.6 days) with the biological window of acute recovery before complete absorption confirms the feasibility of this approach to the production of self-working and battery-free implants, eliminating the need for secondary surgical interventions. Although this study establishes a rigorous predictive framework, the transition to clinical application requires addressing some limitations .First, current simulations assume tissue homogenization, so future work will focus on in vivo bio-verification to address physiological variability and movement abnormalities. Secondly, although fibrin silk ensures biocompatibility, long-term hydrolysis tests are necessary to verify the stability of the Mexin capsule under varying pH conditions. Thirdly, to mitigate signal fluctuations caused by inductive misalignment during patient movement, machine learning (ML) algorithms will be integrated into the external reader to enable automatic dynamic compensation.

Credit Authorship Contribution Statement

Z.H. AL-Araji: Conceptualization, Methodology, Software, Investigation, Writing - original draft. N. Swaikat: Conceptualization, Validation, Formal analysis, Writing - review & editing. All authors have read and agreed to the published version of the manuscript.

Declaration of Competing Interest

The authors declare that they have no known competing financial interests or personal relationships that could have appeared to influence the work reported in this paper.

REFERENCES

Al-Araji, Z.H., 2025. In-chip artificial intelligence technology for generating and self-correcting the topology of low-consumption RC filters. *Engineering and Technology Journal*, 43(8), pp. 705–715. https://etj.uotechnology.edu.iq/article_189015.html

Al-Araji, Z.H., Almawlawe, M.D.H., and Wali, M.H., 2025. Comprehensive characterization of switching and conduction losses in high-ratio step-down converters for next-generation electric vehicles. *Sustainable Engineering and Innovation*, 7(2), pp. 449–462. https://doi.org/10.37868/sei.v7i2.id633

Al-Araji, Z.H., El-Hami, A., and Hussain, M.A., 2021. Methodology for predicting the optimum design of radio-electronic devices. *4th International Conference on Advanced Communication Technologies and Networking (CommNet)*. IEEE. https://ieeexplore.ieee.org/document/9642007

Boutry, C.M., Kaizawa, Y., Hallett, B.C., Loh, M.G., Huang, N.I., Behn, B.C., Tok, J.B.H., Bao, Z., and Chang, J., 2019. Biodegradable and flexible arterial-pulse sensor for the wireless monitoring of blood flow. *Nature Biomedical Engineering*, 3(1), pp. 47–57. https://doi.org/10.1038/s41551-018-0336-5

Chen, Y., Lu, S., Zhang, S., Li, Y., Qu, Z., Chen, Y., Lu, B., Wang, X., and Feng, X., 2022. Recent advances in wireless passive sensors for biomedical health monitoring. *Biosensors*, 12(6), P. 376. https://doi.org/10.3390/bios12060376

Derakhshandeh, H., Kashaf, S.S., Aghabaglou, F., Ghananeel, I.O., and Tamayol, A., 2018. Smart bandages: The future of wound care. *Trends in Biotechnology*, 36(12), pp. 1259–1274. https://doi.org/10.1016/j.tibtech.2018.07.007

Dong, R., Liu, C., Wang, J., Yang, J., Wu, S., and Tang, B.Z., 2024. Recent developments in implantable chemical sensors using flexible, biodegradable materials for biomedical applications. *ACS Nano*, 18(5), pp. 4015–4046. https://doi.org/10.1021/acsnano.3c09999

Gao, Y., Nguyen, D.T., Yeo, T., Lim, S.B., Tan, M.C., and Ho, J.S., 2023. Advances in wearable biosensors for wound healing and infection monitoring. *Biosensors*, 13(3), P. 399. https://doi.org/10.3390/bios13030399

Ghaffar, F.A., Khalid, M., Salama, K.N., and Shamim, A., 2015. Equivalent circuit modeling of implantable antennas for biomedical applications. *IEEE Antennas and Wireless Propagation Letters*, 14, pp. 1234–1238. https://doi.org/10.1109/LAWP.2015.2400325

Guo, Y., Zhong, M., Fang, Z., Wan, P., and Yu, G., 2018. Ti3C2Tx MXene-based flexible piezoresistive sensors. *ACS Nano*, 12(11), pp. 11316–11324. https://doi.org/10.1021/acsnano.8b05927

Gurtner, G.C., Werner, S., Barrandon, Y., and Longaker, M.T., 2008. Wound repair and regeneration. *Nature*, 453(7193), pp. 314–321. https://doi.org/10.1038/nature07039

Huang, K., Li, Z., Lin, J., Han, G., and Huang, P., 2019. Biocompatibility of MXene nanosheets for biomedical applications. *ACS Applied Bio Materials*, 2(11), pp. 4648–4658. https://doi.org/10.1021/acsabm.9b00685

Hwang, S.-W., Tao, H., Kim, D.-H., Cheng, H., Song, J.-K., Rill, E., Brenckle, M.A., Panilaitis, B., Won, S.M., Kim, Y.-S., Song, Y.M., Yu, K.J., Ameer, A., Huang, Y., Hu, J.S., and Rogers, J.A., 2012. A physically transient form of silicon electronics. *Science*, 337(6102), pp. 1640–1644. https://doi.org/10.1126/science.1226319

Kalasin, S., Sangnuang, P., and Khunkaewla, P., 2021. Machine learning-assisted wearable sensor systems for health monitoring. *ACS Applied Electronic Materials*, 3(10), pp. 4235–4246. https://doi.org/10.1021/acsaelm.1c00678

Li, F., Song, Z., Zhao, H., Fan, Y., Yang, G., and Yan, Z., 2021. Highly sensitive and stable humidity sensor based on MXene/AgNWs utilizing Schottky junction. *Sensors and Actuators B: Chemical*, 344, P. 130176. https://doi.org/10.1016/j.snb.2021.130176

Li, G., Fu, J., Nie, B., Zhao, H., and Rogers, J.A., 2022. Recent advances in transient electronics: Materials, devices, and applications. *InfoMat*, 4(5), P. e12297. https://doi.org/10.1002/inf2.12297

Lin, H., Wu, J., and Zhang, L., 2021. Biodegradable electronics: Toxicity, biocompatibility, and environmental impact. *Advanced Science*, 8(15), P. 2100652. https://doi.org/10.1002/advs.202100652

Lonini, L., Dai, A., Shaw,en, N., Mamidi, T., Santoso, F., Schreier, C., Frogner, R., Jayaraman, A., Mummidisetty, C.K., and Rogers, J.A., 2018. Monitor healing of surgical wounds: A review. *IEEE Reviews in Biomedical Engineering*, 11, pp. 22–35. https://doi.org/10.1109/RBME.2018.2820120

Ma, Y., Liu, N., Li, L., Liao, X., Chen, J., Xue, J., Yap, C.C., Wang, Y., and Zhao, C., 2020. Highly flexible and sensitive piezoresistive sensor based on MXene composite sponge for wearable human-machine signals sensing. *Advanced Functional Materials*, 30(4), P. 1907260. https://doi.org/10.1002/adfm.201907260

Mirbozorgi, S.A., Bahrami, H., Sawan, M., Rusche, K., and Gosselin, B., 2016. A smart cage with wireless power transmission and data telemetry for long-term behavioral experiments. *IEEE Transactions on Biomedical Circuits and Systems*, 10(3), pp. 662–672. https://doi.org/10.1109/TBCAS.2015.2414276

Mostafalu, P., Tamayol, A., Rahimi, R., Ochoa, M., Khalilpour, A., Kiaee, G., Yazdi, I.K., Bagherifard, S., Dokmeci, M.R., Ziaie, B., Sonkusale, S., and Khademhosseini, A., 2018. Smart bandage for monitoring and treatment of chronic wounds. *Small*, 14(33), P. 1703509. https://doi.org/10.1002/smll.201703509

Murali, G., Modigunta, J.K.R., Park, Y.H., Lee, J.H., and In, I., 2021. MXenes for sensing applications: Current status and prospects. *Materials Today*, 50, pp. 276–302. https://doi.org/10.1016/j.mattod.2021.04.018

Nguyen, T.Q., Atia, M.M., and Tan, E.L., 2019. Wireless passive resonant sensor for monitoring biodegradable implant degradation. *IEEE Sensors Journal*, 19(21), pp. 9970–9977. https://doi.org/10.1109/JSEN.2019.2927237

Pan, C., Li, S., and Wan, P., 2022. Recent advances in biodegradable biomedical magnesium alloy. *Frontiers in Materials*, 9, P. 886092. https://doi.org/10.3389/fmats.2022.886092

RamRakhyani, A.K., Lazzi, G.J., and Hays, G.L., 2011. Design and optimization of resonance-based efficient wireless power delivery systems for biomedical implants. *IEEE Transactions on Biomedical Circuits and Systems*, 5(1), pp. 48–63. https://doi.org/10.1109/TBCAS.2010.2072782

Sim, K., Rao, Z., Zou, Z., Ershad, F., Liao, J., Suo, P., Wang, J., Tang, J., Li, S., and Yu, C., 2019. Metal oxide semiconductor nanomembrane-based soft, unnoticeable multifunctional electronics for wearable human-machine interfaces. *Science Advances*, 5(8), P. eaav9653. https://doi.org/10.1126/sciadv.aav9653

Song, Y., Mukasa, D., Zhang, H., and Gao, W., 2020. Wireless battery-free wearable sweat sensor powered by human motion. *Science Advances*, 6(40), P. eaay9842. https://doi.org/10.1126/sciadv.aay9842

Tan, Q., Luo, T., Wei, T., Liu, J., Lin, L., and Xiong, J., 2020. A wireless passive pressure and temperature sensor for harsh environment applications. *Microsystems & Nanoengineering*, 6(1), pp. 1–11. https://doi.org/10.1038/s41378-019-0115-3

Wang, D., Lin, Y., Hu, D., Chao, M., and Wan, P., 2023. Emerging MXene-based flexible tactile sensors for health monitoring and haptic perception. *Small*, 19(27), P. 2300283. https://doi.org/10.1002/smll.202300283

Witte, F., Kaese, V., Haferkamp, H., Meyer-Lindenberg, A., Wirth, C.J., and Windhagen, H., 2005. In vivo corrosion of four magnesium alloys and the associated bone response. *Biomaterials*, 26(17), pp. 3557–3563. https://doi.org/10.1016/j.biomaterials.2004.09.049

Xu, G., Cheng, C., Liu, Z., Yuan, W., Wu, J., Feng, Y., Zhu, Z., and Rogers, J.A., 2021. Battery-free and wireless smart wound dressing for wound infection monitoring and electrically controlled treatment. *Advanced Functional Materials*, 31(26), P. 2100852. https://doi.org/10.1002/adfm.20190852

Xu, S., Jayaraman, A., and Rogers, J.A., 2019. Soft, wireless electronic systems for continuous monitoring of physiological status. *Nature Electronics*, 2(4), pp. 165–168. https://doi.org/10.1038/s41928-019-0234-y

Yates, D.C., Rodriguez-Villegas, E., and Williams, A.J., 2017. Optimal transmission frequency for ultralow-power short-range radio links in body sensor networks. *IEEE Transactions on Biomedical Engineering*, 64(5), pp. 1068–1076. https://doi.org/10.1109/TBME.2016.2589574

Zhang, Q., Liang, Q., Nandakumar, D.K., Ravi, S.K., Qu, H., Suresh, L., Zhang, X., Zhang, Y., Yang, L., and Ho, G.W., 2020. Wireless, battery-free, flexible, and biodegradable sensors. *Advanced Functional Materials*, 30(29), P. 1909605. https://doi.org/10.1002/adfm.201909605

Zhu, B., Wang, H., Leow, W.R., Cai, Y., Loh, X.J., Han, M.Y., and Chen, X., 2016. Silk fibroin for flexible electronic devices. *Advanced Materials*, 28(22), pp. 4250–4265. https://doi.org/10.1002/adma.201504276

تصميم ونمذجة الدوائر الإلكترونية لمستشعر حيوي لاسلكي من الميكسين قابل للتحلل لمراقبة الجروح العميقة

زينب حسام موسى الاعرجي[1]*, ندى علي سويقات[2]

[1]قسم الفيزياء، كلية العلوم للبنات، جامعة بغداد، بغداد، العراق
[2]جامعة فارونش التقنية الحكومية، فارونش، روسيا الاتحادية

الخلاصة

من أهم تحديات الرعاية الطبية إصابة الجروح بعد الجراحة، وغالبا ما يفشل الفحص البصري التقليدي في اكتشافها مبكرا. يقترح هذا البحث تصميم مبتكر، نظام القياس عن بعد اللاسلكي السلبي للمراقبة غير المتطفلة لعملية التئام الجروح. يدمج النظام دائرة رنين متوافقة حيويا مع مستشعر مقاوم للضغط عالي الحساسية يعتمد على ($Ti_3C_2T_x$) MXene وهو يعمل ضمن النطاق الترددي الصناعي والطبي القياسي (ISM Band) بتردد 13.56 ميجاهرتز. تعتمد آلية الكشف في النظام على مبدأ" تعديل المعاوقة " (تعديل المعاوقة)، والذي ينتج عن التغيرات في مقاومة المستشعر تحت ضغط الأنسجة الفسيولوجية. تم تصميم النظام ومحاكاته باستخدام بيئة بروتيوس لتقييم استجابة التردد. أظهرت النتائج نطاقا ديناميكيا عاليا، حيث سجل النظام جهد خرج ثابتا قدره 863 مللي فولت (−1.28 ديسيبل) خلال مرحلة الاسترداد (Rs =10 k Ω)، مقابل انخفاض حاد إلى 15 مللي فولت (−36.5 ديسيبل) خلال مرحلة الالتهاب (Rs = 100Ω)، مما يشير بشكل فعال إلى ظاهرة "انهيار الإشارة". بالإضافة إلى ذلك، أكد تحليل الحساسية على الأهمية الحاسمة لدقة المكونات، حيث أدى عدم تطابق السعة إلى تحويل تردد الرنين إلى 11.9 ميجاهرتز. تؤكد هذه النتائج قدرة النظام على التمييز بدقة بين الأنسجة السليمة والملتهبة، مما يوفر حلا واعدا للزرع الطبي القابل للتحلل الحيوي والخالي من البطاريات.

الكلمات المفتاحية: إلكترونيات قابلة للتحلل، مكسين $Ti_3C_2T_x$، قياس لاسلكي سلبي عن بعد، غرسات عابرة.